



Applications of phasors to in vitro time-resolved fluorescence measurements

Martin Štefl^a, Nicholas G. James^b, Justin A. Ross^b, David M. Jameson^{b,*}

^aJ. Heyrovský Institute of Physical Chemistry, v.v.i., Academy of Sciences of the Czech Republic, Dolejškova 3, Prague 18223, Czech Republic

^bDepartment of Cell and Molecular Biology, John A. Burns School of Medicine, University of Hawaii, Honolulu, HI 96813, USA

ARTICLE INFO

Article history:

Received 27 July 2010

Received in revised form 5 November 2010

Accepted 7 November 2010

Available online 13 November 2010

Keywords:

Phasor

Frequency domain

Fluorescence lifetimes

Solvent relaxation

FRET

ABSTRACT

The phasor method of treating fluorescence lifetime data provides a facile and convenient approach to characterize lifetime heterogeneity and to detect the presence of excited state reactions such as solvent relaxation and Förster resonance energy transfer. The method uses a plot of $M \sin(\Phi)$ versus $M \cos(\Phi)$, where M is the modulation ratio and Φ is the phase angle taken from frequency domain fluorometry. A principal advantage of the phasor method is that it provides a model-less approach to time-resolved data amenable to visual inspection. Although the phasor approach has been recently applied to fluorescence lifetime imaging microscopy, it has not been used extensively for cuvette studies. In the current study, we explore the applications of the method to in vitro samples. The phasors of binary and ternary mixtures of fluorescent dyes demonstrate the utility of the method for investigating complex mixtures. Data from excited state reactions, such as dipolar relaxation in membrane and protein systems and also energy transfer from the tryptophan residue to the chromophore in enhanced green fluorescent protein, are also presented.

© 2010 Elsevier Inc. All rights reserved.

Fluorescence methodologies are increasingly used in the chemical, physical, and biological sciences. This increase in popularity is due to improved instrumentation as well as novel probe chemistries and, in biological applications, to the introduction of molecular biological methodologies, including recombinant fluorescent proteins. During recent years, the use of fluorescence in analytical applications has grown in importance and is commonly used to detect and characterize sample heterogeneity in many chemical, physical, and biological systems. Examples of such applications in chemistry include analysis of dissolved organic matter (e.g., polycyclic aromatic hydrocarbons) in air particulates [1,2], in human hair [3], in oil and water samples [4], in foods [5], and in coal-derived extracts [6]. Fluorescence heterogeneity analysis has also been applied in studies of nanotechnology [7], surface chemistry [8], and bacteria identification [9], whereas in biological fields fluorescence heterogeneity analysis is important in many areas such as studies of intrinsic protein fluorescence [10,11], biological membranes [12,13], nucleic acids [14], and calcium gradients [15]. Traditional approaches to detecting and evaluating heterogeneous emitting samples include the use of excitation and emission spectra, such

as excitation–emission matrices (EEMs)¹ [16,17], and synchronous scanning methods [18]. In addition to steady state fluorescence parameters, excited state lifetimes are also important in quantification of the nature and extent of sample heterogeneity [19,20]. An interesting recent example of the use of steady state and time-resolved fluorescence to characterize the heterogeneity in a mixture of fluorophores was presented by Smyk et al. [21], who studied the fluorescence from borage oils that contain polyunsaturated fatty acids. The purpose of their study was to establish, using spectroscopic methods as opposed to chromatographic ones, the presence of polyunsaturated fatty acids of varying extents of conjugation.

Excited state lifetimes have traditionally been measured using either the *impulse* or *harmonic* response method, also known as the “time domain” or “frequency domain”, respectively [19,20,22]. In principle, both methods have the same information content because they can be interconverted using Fourier transforms [23]. In the impulse method, the sample is illuminated with a short pulse of light and the intensity of the emission versus time is recorded.

¹ Abbreviations used: EEM, excitation–emission matrix; LED, light-emitting diode; FRET, Förster resonance energy transfer; FLIM, fluorescence lifetime imaging microscopy; EDTA, ethylenediaminetetraacetic acid; DENS, 2-diethylamino-5-naphthalene-sulfonic acid; LAURDAN, 6-dodecanoyl-2-(*N,N*-dimethylamino)naphthalene; IAEDANS, 5-[(2-iodoacetyl)-amino]naphthalene-1-sulfonic acid, sodium salt; DMPC, 1,2-dimyristoyl-*sn*-glycero-3-phosphocholine; EGFP, enhanced green fluorescent protein; SUV, small unilamellar vesicle; FWHM, full-width half-maximum; TNS, 2-*p*-toluidinyl-6-naphthoyl-4'-cyclohexane carboxylic acid; DANCA, 2-dimethylamino-6-naphthoyl-4' cyclohexane carboxylic acid; ANS, 1-anilinonaphthalene-8-sulfonate; UV, ultraviolet.

* Corresponding author. Address: Department of Cell and Molecular Biology, John A. Burns School of Medicine, University of Hawaii, 651 Ilalo Street, Biosciences 222, Honolulu, HI 96813, USA. Fax: +1 808 692 1968.

E-mail address: djameson@hawaii.edu (D.M. Jameson).

Modern laser sources can now routinely generate pulses with widths on the order of picoseconds or shorter. In the harmonic method (also known as the phase and modulation approach), a continuous light source is typically used, such as a CW laser or xenon arc, and the intensity of this light source is modulated sinusoidally at high frequency. Often an electro-optic device, such as a Pockels cell, is used to modulate the light source. Alternatively, light-emitting diodes (LEDs) or laser diodes can be directly modulated [24]. Frequency domain methods have also been realized using the harmonic content of pulsed sources [25,26].

Both the time domain and frequency domain methods provide information on the excited state decay of a fluorophore. Data analysis of a fluorophore with a single lifetime component is straightforward. More sophisticated data analysis, such as fitting to a specific decay model or using the model-independent maximum entropy method [27], is required when the emission is heterogeneous. Emission heterogeneity could be due to the presence of multiple fluorophores (each giving rise to different exponential decays), excited state processes (e.g., solvent relaxation or Förster resonance energy transfer [FRET]), or nonexponential decays due to processes such as transient quenching. Models used to fit multi-exponential decays are usually based on discrete exponential components or continuous distribution functions [10,19,20]. An alternative model-less approach to fluorescence lifetime determinations, called the phasor plot method, was introduced in 1984 by Jameson et al. [28]. A few years later, the phasor approach was used to correct phase and modulation lifetime measurements for background fluorescence [29]. The phasor approach to fluorescence lifetime analysis was largely dormant until recently, when several laboratories resurrected this approach and applied it to microscopy, for example, for studies on live cells using fluorescence lifetime imaging microscopy (FLIM) [30–36]. These FLIM/phasor studies (also termed AB or polar plots) have largely been focused on FRET systems, although recently they have been applied to study and characterize cell autofluorescence [37]. The phasor approach has not, however, been used extensively for cuvette studies, although some quenching studies in cuvettes have appeared [38]. In the current study, and in an accompanying article, we explore the application of the phasor method to cuvette studies and demonstrate its ability to evaluate and characterize fluorescence heterogeneity with in vitro samples to distinguish excited state reactions and to monitor photophysical processes.

Experimental

Brief theory of frequency domain fluorometry

In frequency domain fluorometry, a continuous wave light source, such as a laser or xenon arc lamp with a Pockels cell or directly modulating LED or laser diodes, is typically used to excite the sample; this light source is sinusoidally modulated at high frequencies (typically from hundreds of kHz to hundreds of MHz) such that the excitation intensity is described by

$$E(t) = E(0)[1 + M_E \sin(\omega t)], \quad (1)$$

where $E(t)$ and $E(0)$ are the excitation intensities at times t and 0 , respectively, M_E is the modulation of the excitation ($M_E = AC_E/DC_E$), and ω is the angular modulation frequency (equal to $2\pi f$, where f is the modulation frequency). The fluorescence emission will then consist of an intensity that is also sinusoidally modulated having the same frequency as the excitation light but shifted in phase and demodulated. If the fluorescence decay is a single exponential, $e^{-t/\tau}$, where τ is the fluorescence lifetime, the sinusoidal fluorescence emission is described by

$$F(t) = F(0)[1 + M_F \sin(\omega t + \phi)], \quad (2)$$

where $F(t)$ and $F(0)$ are the fluorescence intensity at times t and 0 , respectively, M_F is the modulation of the fluorescence ($M_F = AC_F/DC_F$), and ϕ is the phase delay of the fluorescence emission. The measured components in the frequency domain are the phase delay between excitation and emission (ϕ) and the demodulation, which can be related to the lifetime using the following equations:

$$\tan \phi = \omega \tau_p \quad (3)$$

$$M = M_F/M_E = (1 + \omega^2 \tau_m^2)^{-1/2}, \quad (4)$$

where τ_p and τ_m are the phase and modulation lifetimes, respectively. For a fluorescent system that has only a single lifetime, these values will be identical. In the case of a system with multiple lifetimes, the measured τ_p will be less than the measured τ_m . The relationship between ϕ and squared amplitude (M^2) for a mixture of sinusoidal components is described below (the derivations can be found in Refs. [23,39]):

$$\tan \phi = \frac{\sum f_i M_i \sin \phi_i}{\sum f_i M_i \cos \phi_i} \quad (5)$$

$$M^2 = \left(\sum f_i M_i \sin \phi_i \right)^2 + \left(\sum f_i M_i \cos \phi_i \right)^2, \quad (6)$$

where f_i is the fractional photocurrent of the i th component with modulation M_i and phase ϕ_i . (Note that in the case of frequency domain measurements, the intensity fraction corresponds to the fraction of the photocurrent at the particular modulation frequency used and should not be confused with the preexponential function typically used in time domain fluorometry.)

Phasor plots

Jameson et al. [28] described a method of graphically representing phase and modulation data that we have redrawn in Fig. 1A. In

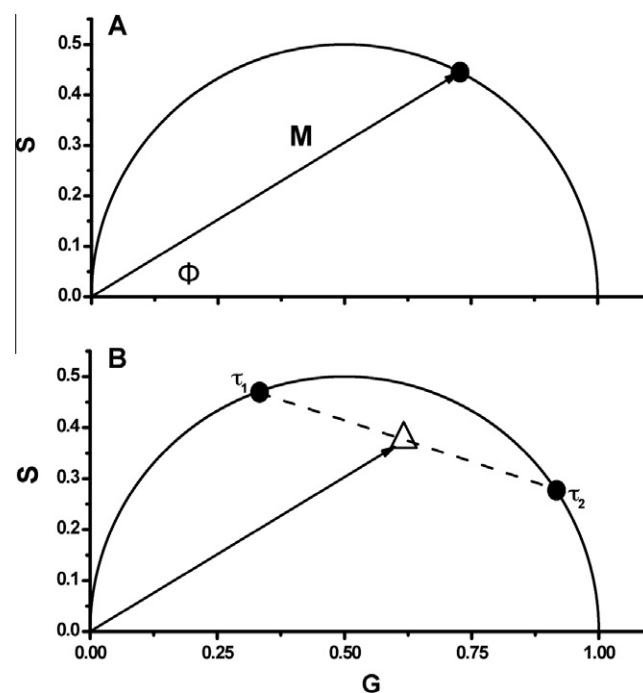


Fig. 1. (A) Schematic illustration of the basic concepts of phasor plots. (B) Two different fluorophores with lifetimes τ_1 and τ_2 , where $\tau_1 > \tau_2$, and their hypothetical mixtures. The dashed line represents the set of mixtures. The solid line illustrates vector M with phase shift ϕ , which corresponds to the mixture, where the ratio of the fluorescence contributions between both fluorophores is 1:1. Note that increased fluorescence contribution from the fluorophore with fluorescence lifetime τ_1 results in an increased angle ϕ and decreased modulation M and also moves the phasor point closer to that of τ_1 .

this figure, the vector has a length equal to the modulation (M) and makes an angle with the x axis equal to the phase delay (ϕ). The x and y coordinates of this vector are derived from Eqs. (5) and (6), and using Weber's notation [23],

$$x = G = M \cos \phi \quad (7)$$

$$y = S = M \sin \phi. \quad (8)$$

For a single-exponential decay, this vector describes a semicircle of radius $\frac{1}{2}$ with a center at $(1/2, 0)$ due to the relationship

$$M = \cos \phi. \quad (9)$$

Therefore, a fluorophore characterized by a single lifetime will always give rise to a phasor point that falls on this semicircle, typically referred to as the universal circle (Fig. 1A). The phasor points for fluorophores that decay with multiple or nonexponential lifetimes are constrained within the universal circle, as described by Eqs. (7) and (8). The location of the phasor point for heterogeneous emitting systems, or multiple single lifetime fluorophores, is the intensity-weighted average of the separate lifetime decay components as described below (Fig. 1B):

$$G_{\text{tot}} = \sum f_i M_i \cos \phi_i \quad (10)$$

$$S_{\text{tot}} = \sum f_i M_i \sin \phi_i. \quad (11)$$

The derivations of the equations and graphical representation have been described previously [28,29,32,36]. In a system containing two decay components, the phasor point will be located on the line between the individual decay vectors weighted by the intensity of each component. Therefore, lifetime heterogeneity within a system will place the phasor point within the universal circle, as illustrated in Fig. 1B.

Although up to this point the mathematical treatment for converting data to a phasor plot has been given using the frequency domain method (which is the method used in this study), raw data from the time domain method can also be analyzed via phasor plots [35]. The equations used to transform the data to the phasor plot from the raw time domain data, originally presented by Weber [23], are

$$G(\omega) = \int_0^{\infty} I(t) \cos(\omega t) dt \bigg/ \int_0^{\infty} I(t) dt \quad (12)$$

$$S(\omega) = \int_0^{\infty} I(t) \sin(\omega t) dt \bigg/ \int_0^{\infty} I(t) dt,$$

where ω can be chosen as the repetition frequency of the pulsed excitation source or another value that depends on the kinetics of the excited state process under investigation. We have outlined a script in MATLAB that can be used to convert/visualize time domain data as a phasor plot in Appendix A. We note that calculations of phasors from frequency or time domain data are carried out by the Globals for Images (aka Sim FCS) software package from the Laboratory for Fluorescence Dynamics (<http://www.lfd.uci.edu>).

Materials and methods

Materials

Rhodamine B, dimethyl POPOP, Hepes, NaCl, ethylenediamine-tetraacetic acid (EDTA), *p*-terphenyl, fluorescein, spectrophotometric-grade ethanol, and glycerol were purchased from Sigma-Aldrich (St. Louis, MO, USA). 2-Diethylamino-5-naphthalenesulfonic acid (DENS) was synthesized by the method of Weber [40]. 6-Dodecanoyl-2-(*N,N*-dimethylamino)naphthalene (LAURDAN) and 5-[(2-iodoacetyl)-amino]naphthalene-1-sulfonic acid, sodium salt (IAEDANS) were obtained from Invitrogen (Carlsbad, CA, USA). 1,2-Dimyristoyl-*sn*-glycero-3-phosphocholine (DMPC)

was obtained from Avanti Polar Lipids (Alabaster, AL, USA). Enhanced green fluorescent protein (EGFP) was a generous gift from Joseph Albanesi.

Vesicle formation

Small unilamellar vesicles (SUVs) were prepared by mixing DMPC (in chloroform/methanol) with the fluorescent dye LAURDAN dissolved in methanol such that the final concentration of lipids was 1 mM and the dye-to-lipid ratio was approximately 1:200. (The concentration of LAURDAN was determined using a molar extinction coefficient of $20,000 \text{ M}^{-1} \text{ cm}^{-1}$ (362 nm) [41].) The mixture was dried for 10 min under nitrogen and then kept under vacuum for approximately 2 h. The dried lipid film was dissolved in 10 mM Hepes (pH 7.4) with 150 mM sodium chloride and 2 mM EDTA, heated to 30–35 °C, and vortexed for 2 min. The cloudy solution was sonicated for 15 min in a G112 SPIT sonicator bath (Laboratory Supplies, Hicksville, NY, USA), resulting in an optically clear solution. The samples were stored at 4 °C and used within 3 days.

Multifrequency lifetime measurements

Fluorescence lifetime measurements were obtained on a ChronosFD Spectrofluorometer (ISS, Champaign, IL, USA). Fluorophores were excited with a 280-nm LED, a 375-nm laser diode, or a 471-nm laser diode with polarizers on the excitation and emission side set to magic angles [42]. The bandpass filters FF01-280/20-25, F01-375/6-25, and FF01-482/18-25 (Semrock, Rochester, NY, USA) were placed after the corresponding excitation source to eliminate spurious light, and the emission was observed through a 420-, 470-, or 525-nm longpass filter. A circulating water bath (Fisher Scientific, Pittsburgh, PA, USA) was used to maintain the temperature. *p*-Terphenyl dissolved in ethanol (1.05 ns), dimethyl POPOP dissolved in ethanol (1.45 ns), and fluorescein dissolved in 0.01 M NaOH (4.05 ns) were used as lifetime references [20].

TNS decay when bound to apomyoglobin

This section involves the reanalysis of data reported previously [43]. Briefly, lifetime data were obtained on a multifrequency phase and modulation fluorometer [44] with modulation frequencies between 10 and 150 MHz. Samples were excited at 327 nm, and emission was monitored through a 510 (± 2)-nm interference filter (10 nm full-width half-maximum [FWHM]). 2-*p*-Toluidinyl-6-naphthoyl-4'-cyclohexane carboxylic acid (TNS, Molecular Probes, Eugene, OR, USA) was added to apoprotein at a molar concentration of less than 1:50 (probe/protein) to minimize nonspecific binding.

Results and discussion

Mixtures of fluorophores

One of the original motivations of this work was to develop a method that could be used to study mixtures of fluorophores for analytical purposes, that is, to be able to facilitate compare different mixtures in such a way that differences in the fluorophore composition would be readily apparent. As mentioned above, a mixture of two monoexponential fluorophores with different fluorescence lifetimes, or a fluorophore characterized by a multiexponential decay, will produce a phasor point within the universal circle, indicating lifetime heterogeneity. The theoretical basis of the phasor plot analysis indicates that this measured phasor point will be located on a line between the points of the individual fluorophores or single-exponential components. Therefore, when three dyes are

combined in solution, the resulting phasor point should be found constrained within a triangle that has vertices defined by the location of the phasor of the individual dyes. Binary and tertiary fluorophore mixtures were studied using fluorophores in ethanol with widely separated lifetimes, namely DENS (fluorescence lifetime $\tau = 29.9$ ns), IAEDANS ($\tau = 5.3$ ns), and Rhodamine B ($\tau = 1.7$ ns). Fig. 2 shows the phasor data at 20 MHz of each individual fluorophore (black dots), solutions containing a mixture of two dyes (DENS/IAEDANS, DENS/Rhodamine B, and IAEDANS/Rhodamine B), and a mixture of all three dyes. As expected, the individual fluorophore's phasor points are located along the universal circle, whereas the phasor points corresponding to mixtures of any two dyes fall on a line between the points on the universal circle corresponding to the individual dyes. For the mixture of the three dyes, the phasor point is located within the triangle defined by the three dual fluorophore mixture lines. The linearity of the summation of multiple fluorescing species (Eqs. (10) and (11)) makes the phasor method suited to the investigation of complex mixtures. We should note, from Fig. 2, that a quantitative extrapolation of exponentials can be used if the location of one component in a mixture is known. If the phasor point of a binary mixture of single-exponential decays is inside the universal circle, and if one of the single-exponential components is known, then the lifetime value of the second component can be determined from the intercept, on the universal circle, of the line between the mixture and the known phasor point. The fractional contribution of each species can be calculated from the relative distance between the phasor point of the pure species and that of the mixture. This analysis can, in theory, be extended to multiple species with multiple lifetime components provided that enough phasor points have been determined. In other words, for the previous case of a binary mixture where one lifetime value is known, this leaves two unknown quantities (τ_2 and f_2 ; recall that $f_1 = 1 - f_2$) with two independent measurements, resulting in a perfectly determined system of equations. As more unknown quantities arise for more complex samples (with more lifetimes and fractions), more modulation frequencies would be required to determine these additional parameters. However, the errors associated with these measurements can significantly decrease the accuracy of these determinations [45]. We also note that these types of considerations, and the effect of Gaussian lifetime distributions on phasor points, have been discussed by Redford and Clegg [32].

The effect of modulation frequency on the location of the phasor point was also examined. As the modulation frequency is in-

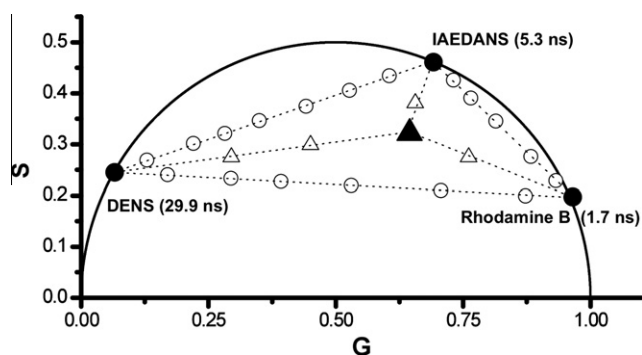


Fig. 2. Phasor data corresponding to ethanol solutions of three fluorophores, each of which is characterized by a single-exponential decay. Closed circles correspond to the individual fluorophores. Open circles between individual fluorophores show the mixture, with changing contributions to the photocurrent, of two particular fluorophores. The closed triangle corresponds to a mixture of all three fluorophores at an equal photocurrent contribution. Increasing the fluorescence contribution of one of the components moves the points closer to the specific corner of the triangle (open triangles). All data were collected at a modulation frequency of 20 MHz and 25 °C.

creased, the measured data should have both a decrease in M and an increase in the Φ , causing the phasor point to move counterclockwise along/within the universal circle. Fig. 3 demonstrates this change in the position of the phasor points for the fluorophore mixtures DENS, IAEDANS, and Rhodamine B when the frequency is increased from 15 MHz (circles) to 30 MHz (triangles). Because frequency domain data are typically obtained using numerous (10–15) modulation frequencies, one can choose among a set of phasor points to find the modulation frequencies that lead to the optimal placement or separation of the phasor points for the particular application. Therefore, the use of widely spaced modulation frequencies could be used in turn to selectively weight one of the fluorescing species in an unknown mixture. Such selection would provide information regarding the phasor locations of each species in the solution.

Dipolar solvent relaxation

In the presence of excited state reactions, such as dipolar solvent relaxation and FRET, phasor data points can fall outside of the universal circle [32]. Alterations in the emission properties of a fluorophore can occur in response to solvent dynamics. In the ground state, fluorophores often have a permanent dipole moment, the strength and direction of which depend on the structure and electronic aspects of the molecule. Immediately after the absorption of a photon, electronic reorganization within the molecule occurs, often resulting in a dipole moment with a different orientation and magnitude. As such, solvent molecules possessing dipoles in proximity to the excited fluorophore dipole are no longer in an equilibrium state and will reorient about the excited state dipole to decrease the energy of the system. If the time of this solvent dipole rearrangement is comparable to or shorter than the excited state lifetime, then solvent reorientation will result in a red shift of the emission, that is, to a lower energy excited state. The time required for the solvent molecules to rearrange depends on the polarity and viscosity of the solvent, with higher viscosity solvents taking longer times to reach their minimum free energy states. In frequency domain fluorometry, solvent relaxation is characterized by an increased phase delay of the emission from the relaxed state relative to emission from the unrelaxed state due to the time it takes for the surrounding solvent molecules to reorient around the newly created excited state fluorophore dipole [46]. This phase delay can result in movement of the phasor point to a position outside of the universal circle. A family of naphthalene-based fluorophores—LAURDAN, and 2-dimethylamino-6-naphthoyl-4'-cyclohexane carboxylic acid (DANCA), designed by Weber

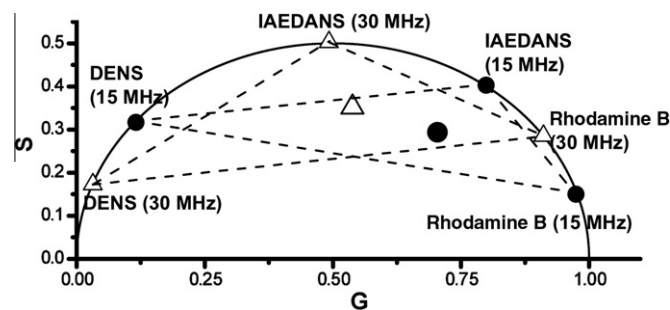


Fig. 3. Frequency dependence on the location of phasor points for DENS, IAEDANS, and Rhodamine B alone and in various mixtures. Circles correspond to individual fluorophores at 15 MHz, whereas triangles correspond to individual fluorophores recorded at 30 MHz. Dashed lines between circles and triangles represent the two-component mixture of varying contributions between corresponding fluorophores. The larger circle and triangle in the middle represent mixtures of all three fluorophores, with an equal contribution to the photocurrent from each, at 15 MHz (circle) and 30 MHz (triangle). All data were measured with 375 nm excitation at 25 °C.

[47]—are characterized by particularly large excited state dipoles, and this renders them well-suited to causing dipolar relaxation in appropriate systems.

Dipolar relaxation in vesicles

Dipolar relaxation can occur in heterogeneous systems such as membranes and proteins where the “solvent” molecules are lipids (or water molecules that penetrate into the lipid phase) and amino acid residues, respectively. In these cases, the presence of relaxation processes can provide an indication of the underlying dynamics of the biomolecule under investigation. An example of such relaxation processes for probes embedded in DMPC SUVs is the emission spectra of LAURDAN over a range of temperatures (data not shown). At temperatures below the transition temperature (23 °C [48]), the emission maximum is approximately 440 nm, whereas at higher temperatures, the maximum shifts to approximately 480 nm. At 30 °C, there is a broad peak from 450 to 475 nm, demonstrating the presence of both gel and liquid crystalline phases. In the case of the LAURDAN/DMPC system, the spectral shifts are attributed to the fact that the liquid crystalline lipid phase allows penetration of the water molecules into the bilayer, which is responsible for the dipolar relaxation mechanism [49,50].

Inspection of the LAURDAN/DMPC phasor plot (Fig. 4) shows that the phasor points corresponding to data collected using the 470-nm filter are completely outside of the universal circle, indicative of a dipolar solvent relaxation mechanism. When the entire LAURDAN emission is collected using the 420-nm longpass filter, the phasor points lay along or very close to the universal circle, indicating that the nonrelaxed emission dominates the observed decay. Using the 470-nm longpass filter, the collected emission is weighted primarily from the molecules that undergo dipolar relaxation and the location of the phasor points outside of the universal circle is more pronounced. However, the points above 25 °C show a clear trend above the universal circle, indicating the presence of an excited state event. We should note that the LAURDAN phasor data presented here support the dipolar relaxation models for LAURDAN/vesicle systems [49,50] as opposed to other models [51]. In principle, the phasor plots allow calculation of the rates of dipolar relaxation processes in such systems, but this analysis is beyond the scope of the current study.

TNS with apomyoglobin

Fluorescent molecules, such as 1-anilinoanthracene-8-sulfonate (ANS), TNS, and DANCA, have been used in a number of protein systems to investigate dynamic characteristics of the protein matrix [43,52–54]. In the excited state, the dipole moments of such fluorophores associated with proteins can cause rearrange-

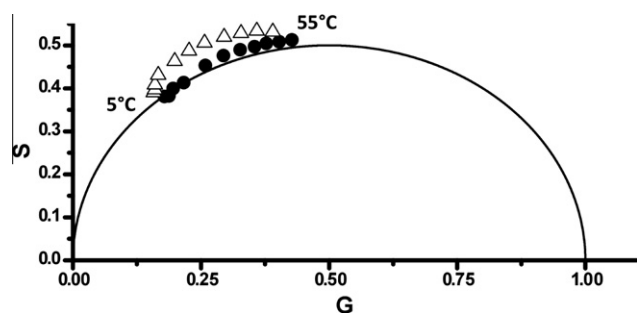


Fig. 4. LAURDAN in DMPC vesicles. Circles and triangles represent data collected for temperatures between 5 °C (left) and 55 °C (right), with 5 °C intervals, at modulation frequencies of 55 MHz (circles) and 57 MHz (triangles). Excited at 375 nm; emission was viewed through 420-nm (circles) and 470-nm (triangles) longpass filters.

ments of charges and dipoles in the protein matrix, for example, due to charged or polar amino acid side chains or even the dipoles associated with the peptide bonds. If the dynamics of the protein allows for dipolar relaxation of the protein matrix, then distinct alterations in the fluorophore's emission properties can result, analogous to the case of dipolar relaxation of solvent molecules described above. Bismuto et al. [43] compared the emission properties of TNS associated with both sperm whale and tuna apomyoglobin to ascertain whether this probe revealed differences in the heme-binding sites of these phylogenetically related proteins. In the original publication, it was documented that the phase and modulation lifetimes for TNS/tuna myoglobin decreased with increasing frequencies, indicative of heterogeneous emitting population, whereas for TNS/sperm whale myoglobin the phase lifetime became longer than the modulation lifetime with increasing frequency (going negative at the highest frequency). This latter case was concluded to be an excited state reaction, specifically dipolar relaxation within the heme-binding pocket. Time-resolved data could not detect the presence of dipolar relaxation in TNS/tuna myoglobin despite steady state fluorescence data that suggested its presence. The authors concluded that although dipolar relaxation is likely occurring in both proteins, the structural heterogeneity in the heme-binding pocket of tuna myoglobin produces some microenvironments that are not favorable to dipolar relaxation of the TNS molecule.

The phase and modulation data of TNS with apomyoglobin from Bismuto et al.'s study [43] are reproduced in Fig. 5 using the phasor approach. The resultant phasor plot shows distinct differences between the two data sets, with the tuna TNS/apomyoglobin data entirely within the universal circle. TNS in a homogeneous isotropic solvent decays with a single exponential; thus, the multiexponential decay of the tuna apomyoglobin is suggestive of different populations, and hence lifetime heterogeneity, of local probe environments. Although there may be dipolar relaxation in this system, the lifetime heterogeneity keeps the phasor points within the universal circle. In the case of TNS bound to sperm whale apomyoglobin, however, many of the phasor points are outside of the universal circle, and hence an excited state reaction, attributed to dipolar relaxation, is evident. The heterogeneity in the phasor points of TNS/tuna myoglobin suggests multiple conformations of TNS when bound as compared with when bound to sperm whale myoglobin. Thus, it can be concluded that there is more flexibility in the pocket of tuna myoglobin. These conclusions are in line with those made by Bismuto et al. [43].

Energy transfer

FRET is one of the most popular fluorescence techniques in the biological sciences [19,20]. Unlike the crystallographic technique,

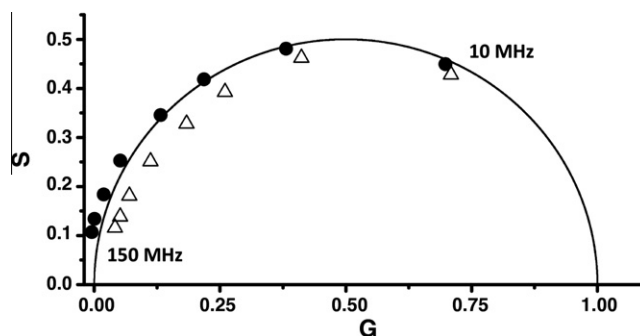


Fig. 5. Phasor data for sperm whale TNS/apomyoglobin (circles) and tuna TNS/apomyoglobin (triangles) adducts (modulation frequencies from 10 to 150 MHz [right to left]). Phase and modulation data were taken from Ref. [43].

FRET can provide structural information rapidly and facily in solution, at low concentrations, and has the potential to report on intermediate or short-lived conformations of proteins [55,56]. Changes in the fluorescence emission from a donor molecule, measured by either the steady state or time-resolved method, in the absence and presence of an acceptor fluorophore (either different from or identical to the donor) can, in turn, be used to estimate distances [19], although the method is subject to caveats such as the precise orientation of donor and acceptor. FRET between a donor, with a single lifetime component, and an acceptor molecule will result in a shortening of the donor lifetime. In a phasor plot, this circumstance will cause the phasor point of the donor to move along the universal circle [35,57]. If there is an unequal ratio of donor to acceptor (donor > acceptor), then a small number of donors will maintain the original lifetime, producing a heterogeneous decay. Phasor analysis of such a sample would produce a point with a shorter average lifetime than the donor alone; however, the point would fall inside the universal circle. Alternatively, the acceptor decay can be monitored through direct excitation or through transfer from an excited donor. Any difference between the phasor points of the acceptor, directly excited or from donor transfer, would be the result of energy transfer. The decay from the acceptor, after energy transfer, should be longer than if the acceptor were directly excited due to the time delay from absorption by the donor, energy transfer between the donor/acceptor pair, and the subsequent emission from the acceptor. This delay is manifested as a lengthening of the measured phase, and such a delay will move the phasor point outside of the universal circle (see, e.g., Refs. [57,58]). Fig. 6 shows the phasor points associated with the visible emission (>525 nm) from EGFP, excited with both visible (471 nm) and ultraviolet (UV, 280 nm) excitation, as a function of modulation frequency (16–300 MHz). As is evident for the phasor plot, 471 nm excitation results in phasor points corresponding to single-exponential decays; that is, the points are all on the universal circle. On the other hand, 280 nm excitation, which will directly excite the single tryptophan residue (as well as the tyrosine residues) in addition to some direct excitation of the EGFP chromophore, results in phasor points that are all outside of the universal circle. Hence, although some of the visible chromophores may be directly excited at 280 nm, there is enough tryptophan-to-chromophore energy transfer to move the phasor point outside of the universal circle. This observation is consistent with the observation by Visser et al. [59] on energy transfer in a fluorescent protein. This demonstration illustrates the utility of the phasor method to visualize photophysical processes and to provide insights into excited state kinetics that are often difficult to obtain by other methods. We note that FRET efficiencies can also be calculated, in principle, from phasor data; the Globals for Images (aka Sim FCS) software mentioned earlier carries out these calculations.

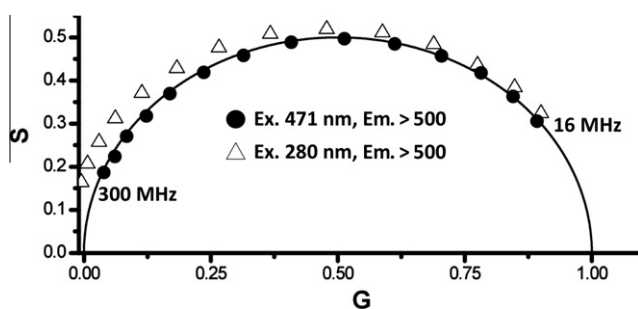


Fig. 6. Decay data of EGFP excited at 471 nm (circles) and 280 nm (triangles). All of the data recorded with 280 nm excitation fall outside of the universal circle, an indication of an excited state process, allowing a simple visualization of the energy transfer process between the lone tryptophan (donor) and the EGFP chromophore (acceptor).

Reproducibility

We established, through simulations, data, and test samples, that in our instrument the statistical errors between individual phasor measurements are on the order of ± 0.005 for both G and S values (data not shown). We can then have confidence that movement of the phasor point by approximately 0.01 on the G or S axis constitutes a statistically significant change.

Conclusion

We have demonstrated that the extension of the phasor method from FLIM to cuvette measurements provides a method that complements other approaches and that, in some cases, provides insights that would otherwise be difficult to obtain. In particular, the method allows facile analysis of sample heterogeneity and ready identification of excited state processes such as dipolar relaxation and FRET. In our next article, we will specifically demonstrate the application of the phasor method to protein studies, including protein–ligand and protein–protein interactions as well as protein unfolding.

Acknowledgments

This work was supported in part by funding from Allergan and from National Institutes of Health Grant RO1GM076665 (D.M.J.). M. Štefl was supported by the Ministry of Education of the Czech Republic via Grant LC06063 and by Charles University in Prague via Fond Mobility. We thank Joseph Albanesi for supplying the EGFP.

Appendix A. Conversion of time domain data to phasors

Throughout the article, we describe how raw data from frequency domain measurements can be converted to phasor plots. Yet raw data from both time domain and frequency domain lifetime measurements can be converted to phasor plots. We have outlined lines of code (below), which can be used in MATLAB, for the conversion of raw time domain data into a phasor plot. We also note that the software package Globals for Images (aka Sim FCS), available from the Laboratory for Fluorescence Dynamics (<http://www.lfd.uci.edu>), can use frequency or time domain data to construct phasor plots.

```
function [G,S] = plottscpcphasor(decay,ref,ref_tau,freq,delta_t)
%decay is the array of the decay curve from TCSPC
%ref is the decay curve of the reference or IRF curve
%ref_tau is the lifetime of the reference compound (zero for IRF)
%freq is the freq domain freq you want to use to plot the phasor
%delta_t is the size (time) of each of the bins of the decay curve
w=2*pi*freq;
%calculate ref phasor
Gn_ref=0;
Sn_ref=0;
area_ref=0;
for bin = 1:length(ref)-1
    Gn_ref = Gn_ref + ref(bin).*cos(w*delta_t.*(bin-.5))*delta_t;
    Sn_ref = Sn_ref + ref(bin).*sin(w*delta_t.*(bin-.5))*delta_t;
    area_ref = area_ref + (ref(bin)+ref(bin+1)).*delta_t./2;
end
G_ref = Gn_ref./area_ref;
S_ref = Sn_ref./area_ref;
%calculate phase and modulation corrections
M_ref = (1 + (w*ref_tau).^2).^(-0.5);
ph_ref = atan(w*ref_tau);
```

```

M_cor = sqrt(G_ref.^2+S_ref.^2)./M_ref;
ph_cor = -atan2(S_ref,G_ref)+ph_ref;
%calculate data phasor
Gn=0;
Sn=0;
area=0;
for bin = 1:length(decay)-1
    Gn = Gn + decay(bin).*cos(w*delta_t.*(bin-.5)).^delta_t;
    Sn = Sn + decay(bin).*sin(w*delta_t.*(bin-.5)).^delta_t;
    area = area + (decay(bin) + decay(bin+1)).*delta_t./2;
end
Gdec = Gn./area;
Sdec = Sn./area;
G = (Gdec.*cos(ph_cor) - Sdec.*sin(ph_cor))./M_cor;
S = (Gdec.*sin(ph_cor) + Sdec.*cos(ph_cor))./M_cor;
%Plot phasor point and universal circle
theta = 0:0.01:pi;
plot(0.5+0.5*cos(theta),0.5*sin(theta));
axis([0 1 0 1]);
axis square;
hold on;
xlabel('G')
ylabel('S')
plot(G,S,'b')

```

The above code calculates the phasor location of a known reference decay curve or the instrument response function (IRF) and then determines the transformation of the point to the appropriate phasor point ((1,0) for the IRF). This transformation consists of a correction to the amplitude (modulation) and a rotation about the origin (phase). The reference decay curve is the complete decay curve of a compound with a known single-exponential lifetime, for example, fluorescein in 0.01 M NaOH (4.05 ns) or *p*-terphenyl in ethanol (1.05 ns). Note that, unlike the background subtraction method in the frequency domain, this correction method is *not* an addition or subtraction of a phasor vector but rather a rotation and rescaling of the phasor.

References

- [1] M. Akyuz, H. Cabuk, Particle-associated polycyclic aromatic hydrocarbons in the atmospheric environment of Zonguldak, Turkey, *Sci. Total Environ.* 405 (2008) 62–70.
- [2] Y. Hashi, T.R. Wang, W. Du, J.M. Lin, Rapid and sensitive determination of polycyclic aromatic hydrocarbons in atmospheric particulates using fast high-performance liquid chromatography with on-line enrichment system, *Talanta* 74 (2008) 986–991.
- [3] A. Toriba, Y. Kuramae, T. Chetiyankornkul, R. Kizu, T. Makino, H. Nakazawa, K. Hayakawa, Quantification of polycyclic aromatic hydrocarbons (PAHs) in human hair by HPLC with fluorescence detection: a biological monitoring method to evaluate the exposure to PAHs, *Biomed. Chromatogr.* 17 (2003) 126–132.
- [4] S.A. Bortolato, J.A. Arancibia, G.M. Escandar, Non-trilinear chromatographic time retention–fluorescence emission data coupled to chemometric algorithms for the simultaneous determination of 10 polycyclic aromatic hydrocarbons in the presence of interferences, *Anal. Chem.* 81 (2009) 8074–8084.
- [5] R. Rodríguez-Acuna, C. Perez-Camino Mdel, A. Cert, W. Moreda, Sources of contamination by polycyclic aromatic hydrocarbons in Spanish virgin olive oils, *Food Addit. Contam. A* 25 (2008) 115–122.
- [6] T. Katoh, S. Yokoyama, Y. Sanada, Analysis of a coal-derived liquid using high-pressure liquid chromatography and synchronous fluorescence spectrometry, *Fuel* 59 (1980) 845–850.
- [7] D. Tasis, J. Mikroyannidis, V. Karoutsos, C. Galiotis, K. Papagelis, Single-walled carbon nanotubes decorated with a pyrene–fluorenevinylene conjugate, *Nanotechnology* 20 (2009) 135606.
- [8] W.B. Williams, B.A. Mullany, W.C. Parker, P.J. Moyer, M.H. Randles, Using quantum dots to tag subsurface damage in lapped and polished glass samples, *Appl. Opt.* 48 (2009) 5155–5163.
- [9] H. Bhatta, E.M. Goldys, R.P. Learmonth, Use of fluorescence spectroscopy to differentiate yeast and bacterial cells, *Appl. Microbiol. Biotechnol.* 71 (2006) 121–126.
- [10] J.A. Ross, D.M. Jameson, Time-resolved methods in biophysics: 8. Frequency domain fluorometry—applications to intrinsic protein fluorescence, *Photochem. Photobiol. Sci.* 7 (2008) 1301–1312.
- [11] N.G. James, J.A. Ross, A.B. Mason, D.M. Jameson, Excited-state lifetime studies of the three tryptophan residues in the N-lobe of human serum transferrin, *Protein Sci.* 19 (2009) 99–110.
- [12] T. Parasassi, F. Conti, E. Gratton, O. Saporita, Membranes modification of differentiating proerythroblasts: variation of 1,6-diphenyl-1,3,5-hexatriene lifetime distributions by multifrequency phase and modulation fluorimetry, *Biochim. Biophys. Acta* 898 (1987) 196–201.
- [13] R. Fiorini, M. Valentino, S. Wang, M. Glaser, E. Gratton, Fluorescence lifetime distributions of 1,6-diphenyl-1,3,5-hexatriene in phospholipid vesicles, *Biochemistry* 26 (1987) 3864–3870.
- [14] R.M. Clegg, A.I. Murchie, A. Zechel, C. Carlberg, S. Diekmann, D.M. Lilley, Fluorescence resonance energy transfer analysis of the structure of the four-way DNA junction, *Biochemistry* 31 (1992) 4846–4856.
- [15] A. Celli, S. Sanchez, M. Behne, T. Hazlett, E. Gratton, T. Mauro, The epidermal Ca²⁺ gradient: measurement using the phasor representation of fluorescent lifetime imaging, *Biophys. J.* 98 (2010) 911–921.
- [16] G. Weber, Enumeration of components in complex systems by fluorescence spectrophotometry, *Nature* 190 (1961) 27–29.
- [17] J. Chen, A. Lee, J. Zhao, H. Wang, H. Lui, D.I. McLean, H. Zeng, Spectroscopic characterization and microscopic imaging of extracted and in situ cutaneous collagen and elastic tissue components under two-photon excitation, *Skin Res. Technol.* 15 (2009) 418–426.
- [18] R.J. Kavanagh, B.K. Burnison, R.A. Frank, K.R. Solomon, G. Van Der Kraak, Detecting oil sands process-affected waters in the Alberta oil sands region using synchronous fluorescence spectroscopy, *Chemosphere* 76 (2009) 120–126.
- [19] B. Valeur, *Molecular Fluorescence*, Wiley-VCH, Weinheim, Germany, 2002.
- [20] J. Lakowicz, *Principles of Fluorescence Spectroscopy*, Springer, New York, 2006.
- [21] B. Smyk, R. Amarowicz, M. Szabelski, I. Gryczynski, Z. Gryczynski, Steady-state and time-resolved fluorescence studies of stripped borage oil, *Anal. Chim. Acta* 646 (2009) 85–89.
- [22] F.V. Bright, T.A. Betts, K.S. Litwiler, Advances in multifrequency phase and modulation fluorescence analysis, *Crit. Rev. Anal. Chem.* 21 (1990) 389–405.
- [23] G. Weber, Resolution of the fluorescence lifetimes in a heterogeneous system by phase and modulation measurements, *J. Phys. Chem.* 85 (1981) 949–953.
- [24] B. Barbieri, E. Terpetschnig, D.M. Jameson, Frequency-domain fluorescence spectroscopy using 280-nm and 300-nm light-emitting diodes: measurement of proteins and protein-related fluorophores, *Anal. Biochem.* 344 (2005) 298–300.
- [25] E. Gratton, D.M. Jameson, N. Rosato, G. Weber, Multifrequency cross-correlation phase fluorometer using synchrotron radiation, *Rev. Sci. Instrum.* 55 (1984) 486–494.
- [26] J.R. Alcalá, E. Gratton, F.G. Prendergast, Fluorescence lifetime distributions in proteins, *Biophys. J.* 51 (1987) 597–604.
- [27] J.C. Brochon, Maximum entropy method of data analysis in time-resolved spectroscopy, *Methods Enzymol.* 240 (1994) 262–311.
- [28] D.M. Jameson, E. Gratton, R.D. Hall, The measurement and analysis of heterogeneous emissions by multifrequency phase and modulation fluorimetry, *Appl. Spectrosc. Rev.* 20 (1984) 55–106.
- [29] G.D. Reinhart, P. Marzola, D.M. Jameson, E. Gratton, A method for on-line background subtraction in frequency domain fluorometry, *J. Fluoresc.* 1 (1991) 153–162.
- [30] A.H. Clayton, Q.S. Hanley, D.J. Arndt-Jovin, V. Subramaniam, T.M. Jovin, Dynamic fluorescence anisotropy imaging microscopy in the frequency domain (rFLIM), *Biophys. J.* 83 (2002) 1631–1649.
- [31] A.H.A. Clayton, Q.S. Hanley, P.J. Verwee, Graphical representation and multicomponent analysis of single-frequency fluorescence lifetime imaging microscopy data, *J. Microsc.* 213 (2004) 1–5.
- [32] G.I. Redford, R.M. Clegg, Polar plot representation for frequency-domain analysis of fluorescence lifetimes, *J. Fluoresc.* 15 (2005) 805–815.
- [33] Q.S. Hanley, A.H.A. Clayton, AB-plot assisted determination of fluorophore mixtures in a fluorescence lifetime microscope using spectra or quenchers, *J. Microsc.* 218 (2005) 62–67.
- [34] A. Esposito, H.C. Gerritsen, T. Oggier, F. Lustenberger, F.S. Wouters, Innovating lifetime microscopy: a compact and simple tool for life sciences, screening, and diagnostics, *J. Biomed. Opt.* 11 (2006) 34016.
- [35] M.A. Digman, V.R. Caiola, M. Zamai, E. Gratton, The phasor approach to fluorescence lifetime imaging analysis, *Biophys. J.* 94 (2008) L14–L16.
- [36] A.H.A. Clayton, The polarized AB plot for the frequency-domain analysis and representation of fluorophore rotation and resonance energy homotransfer, *J. Microsc.* 232 (2008) 306–312.
- [37] C. Stringari, M. Digman, P. Donovan, E. Gratton, Multiple components mapping of live tissue by phasor analysis of fluorescence lifetime imaging, *Biophys. J.* 98 (2010) 2144.
- [38] G.I. Redford, Z.K. Majumdar, J.D. Sutin, R.M. Clegg, Properties of microfluidic turbulent mixing revealed by fluorescence lifetime imaging, *J. Chem. Phys.* 123 (2005) 224504.
- [39] F.W.J. Teale, Phase and modulation fluorometry, in: R.B. Cundall, R.E. Dale (Eds.), *Time-Resolved Fluorescence Spectroscopy in Biochemistry and Biology*, Plenum, New York, 1983, pp. 59–80.
- [40] G. Weber, Polarization of the fluorescence of macromolecules: II. Fluorescent conjugates of ovalbumin and bovine serum albumin, *Biochem. J.* 51 (1952) 155–167.

- [41] T. Parasassi, F. Conti, E. Gratton, Time-resolved fluorescence emission spectra of Laurdan in phospholipid vesicles by multifrequency phase and modulation fluorometry, *Cell. Mol. Biol.* 32 (1986) 103–108.
- [42] R.D. Spencer, G. Weber, Influence of Brownian rotations and energy transfer upon the measurements of fluorescence lifetime, *J. Chem. Phys.* 52 (1970) 1654–1663.
- [43] E. Bismuto, G. Irace, G. Colonna, D.M. Jameson, E. Gratton, Dynamic aspects of the heme-binding site in phylogenetically distant myoglobins, *Biochim. Biophys. Acta* 913 (1987) 150–154.
- [44] E. Gratton, M. Limkeman, A continuously variable frequency cross-correlation phase fluorometer with picosecond resolution, *Biophys. J.* 44 (1983) 315–324.
- [45] D.M. Jameson, E. Gratton, Analysis of heterogeneous emissions by multifrequency phase and modulation fluorometry, in: D. Eastwood (Ed.), *New Directions in Molecular Luminescence*, American Society for Testing and Materials, Philadelphia, 1983, pp. 67–81.
- [46] E. Bismuto, D.M. Jameson, E. Gratton, Dipolar relaxations in glycerol: a dynamic fluorescence study of 4-[2'-(dimethylamino)-6'-naphthoyl]cyclohexanecarboxylic acid (DANCA), *J. Am. Chem. Soc.* 109 (1987) 2354–2357.
- [47] G. Weber, F.J. Farris, Synthesis and spectral properties of a hydrophobic fluorescent probe: 6-propionyl-2-(dimethylamino)naphthalene, *Biochemistry* 18 (1979) 3075–3078.
- [48] M. Caffrey, J. Hogan, LIPIDAT: a database of lipid phase transition temperatures and enthalpy changes—DMPC data subset analysis, *Chem. Phys. Lipids* 61 (1992) 1–109.
- [49] T. Parasassi, G. Ravagnan, R.M. Rusch, E. Gratton, Modulation and dynamics of phase properties in phospholipid mixtures detected by Laurdan fluorescence, *Photochem. Photobiol.* 57 (1993) 403–410.
- [50] T. Parasassi, M. Di Stefano, M. Loiero, G. Ravagnan, E. Gratton, Influence of cholesterol on phospholipid bilayers phase domains as detected by Laurdan fluorescence, *Biophys. J.* 66 (1994) 120–132.
- [51] S. Merlo, P. Yager, W. Burgess, An optical method for detecting anesthetics and other lipid soluble compounds, *Sens. Actuators A* 23 (1990) 1150–1154.
- [52] G. Weber, L.B. Young, Fragmentation of bovine serum albumin by pepsin: I. The origin of the acid expansion of the albumin molecule, *J. Biol. Chem.* 239 (1964) 1415–1423.
- [53] L. Stryer, The interaction of a naphthalene dye with apomyoglobin and apohemoglobin: a fluorescent probe of non-polar binding sites, *J. Mol. Biol.* 13 (1965) 482–495.
- [54] A. Gafni, R.P. DeToma, R.E. Manrow, L. Brand, Nanosecond decay studies of a fluorescence probe bound to apomyoglobin, *Biophys. J.* 17 (1977) 155–168.
- [55] H.C. Cheung, I. Gryczynski, H. Malak, W. Wiczak, M.L. Johnson, J.R. Lakowicz, Conformational flexibility of the Cys697–Cys707 segment of myosin subfragment-1: distance distributions by frequency-domain fluorometry, *Biophys. Chem.* 40 (1991) 1–17.
- [56] W.M. Shih, Z. Gryczynski, J.R. Lakowicz, J.A. Spudich, A FRET-based sensor reveals large ATP hydrolysis-induced conformational changes and three distinct states of the molecular motor myosin, *Cell* 102 (2000) 683–694.
- [57] Y.C. Chen, B.Q. Spring, C. Buranachi, B. Tong, G. Malachowski, R.M. Clegg, General concerns of FLIM data representation and analysis, in: A. Periasamy, R.M. Clegg (Eds.), *FLIM Microscopy in Biology and Medicine*, Chapman & Hall/CRC, Boca Raton, FL, 2010, pp. 291–339.
- [58] Y.C. Chen, R.M. Clegg, Fluorescence lifetime-resolved imaging [review], *Photosynth. Res.* 102 (2009) 143–155.
- [59] N.V. Visser, J.W. Borst, M.A. Hink, A. van Hoek, A.J. Visser, Direct observation of resonance tryptophan-to-chromophore energy transfer in visible fluorescent proteins, *Biophys. Chem.* 116 (2005) 207–212.